社団法人　電子情報通信学会
THE INSTITUTE OF ELECTRONICS,
INFORMATION AND COMMUNICATION ENGINEERS

信学技報
TECHNICAL REPORT OF IEICE.

[Poster Presentation] A study on FFT-ED based signal area estimation for spectrum awareness

Riki MIZUCHI†, Kenta UMEBAYASHI†, Janne J. LEHTOMÄKI††, and Miguel LÓPEZ-BENÍTEZ†††

† Department of Electrical and Electronic Engineering, Tokyo University of Agriculture and Technology, 2–24–16 Naka-cho, Koganei-shi, Tokyo, 184–8588 Japan
†† University of Oulu, P. O. BOX 4500 FIN-90014, University of Oulu, Finland
††† University of Liverpool, Merseyside, L69 3GJ, United Kingdom
E-mail: mizuchi@st.go.tuat.ac.jp

Abstract For achieving 2-layer smart spectrum access (SSA) which corresponds to feasible strategy of DSA, a development of spectrum awareness system (SAS) is required. We focus on a core signal processing in SAS, which is called signal area (SA) estimation. Simple-SA (S-SA) estimation has been developed as a method to find SA, which means occupying area by PU in time-frequency domain. One of the issues of S-SA estimation is that it increases false alarm. In this paper, we propose L-shaped false alarm removal (L-FAR). We analytically derive sub-optimum parameters for L-FAR based on constant false alarm rate (CFAR). Numerical evaluations show the sub-optimum solution can achieve competitive detection performance with the optimum solution. In addition, it is shown that the proposed method can achieve better detection performance compared to the other methods.

Key words Dynamic spectrum access, Spectrum measurement, Smart spectrum access

1. Introduction

Due to fixed spectrum assignment policy and increasing demand of wireless communications, there is little room to accommodate new wireless systems. However, research by Federal Communications Commission (FCC) shows utilization rate of spectrum in terms of time and frequency is in range of 15% to 85% [1]. It means there are a lot of unused spectrum, which is called white space (WS). For this issue, dynamic spectrum access (DSA) [2] has been investigated. In DSA, there are primary users (PUs), which have their own spectrum, and secondary users (SUs), which do not have their own spectrum. SUs correspond to new wireless system. SUs can use the vacant spectrum while the spectrum utilization by SUs does not cause any harmful interference to PUs.

In DSA, SUs have to detect WS properly. Moreover, instantaneous information of WS is necessary to share the spectrum with PUs whose spectrum utilization change dynamically in time such as mobile data communication. Spectrum sensing is a strong approach in such a situation [3]–[5]. However, DSA demands substantially high sensing accuracy and low latency for spectrum sensing to avoid harmful interference to PU. Furthermore, low implementation cost and energy efficient scheme is required since spectrum sensing is implemented to small and low cost mobile terminal [6].

One of the approaches to achieve these requirements is using statistical information of PU's spectrum utilization such as duty cycle (DC) or channel occupancy rate (COR) [7]. These information can be used to enhance spectrum sensing performance [8]–[10]. Moreover, DC and/or COR can be used for more sophisticated spectrum management, channel selection and MAC protocol design to enhance spectrum efficiency [10]–[13].

However, it is difficult to estimate statistical information based on long term observation by SU terminals because of their limitation of energy consumption, i.e. computational cost. 2-layer smart spectrum access (SSA) was proposed as a practical approach to actualize statistical information based DSA [14],[15]. In the 1st layer of 2-layer SSA, SUs can use spatially and/or temporally vacant spectrum easily by utilizing statistical information of PU's spectrum utilization. There is spectrum awareness system (SAS) in the 2nd layer. A role of SAS is to estimate statistical information based on long term, broad spectrum and large area spectrum measurement, and to provide the statistical information to SUs.

2-layer architecture can release SUs from estimation cost of statistical information.

Since we have to cover large area, a large number of spectrum sensors must be spatially deployed. Considering such a production cost, spectrum usage detection in each spectrum sensor is required to be simple and accurate. As shown in Fig. 1, assumed spectrum usage detection consists of 3 processes; Fourier transform, such as Welch fast Fourier transform (FFT), energy detection (ED) and signal area (SA) estimation [15].

ED is a very simple signal detection method and it does not require any prior information of PU signal [16]. FFT based ED (FFT-ED) [17] is also widely investigated in the area of spectrum sensing to sense multiple wireless systems simultaneously. In FFT-ED, sensing result is obtained for each frequency bin. Signal detection performance of ED is not very high as compared to feature detection, matched filter, etc. [3], [5], [6]. On the other hand, Welch FFT based ED (Welch FFT-ED) can improve FFT-ED performance since power spectrum is averaged in time domain to suppress the effect of noise uncertainty at the expense of frequency resolution [15], [18], [19].

Latency requirement of spectrum measurement is not so strict as that of spectrum sensing since the spectrum measurement is used to estimate statistical information based on long term spectrum measurement. Therefore, we can add post process to Welch FFT-ED [15]. Output of Welch FFT-ED is in the form of a two-dimensional time/frequency grid. We denote a single element of the grid corresponding to one time slot and one frequency bin by *tile*. State of tile is $\mathcal{H}_1$ if tile is occupied, or $\mathcal{H}_0$ if tile is unoccupied. The cluster of $\mathcal{H}_1$ tiles is referred to SA and SA in digital wireless communication is typically rectangular shape. This aspect can provide diversity gain by exploiting the correlation among neighboring tile's state. This process is denoted by SA estimation.

There were similar approaches; localization algorithm based on double-thresholding (LAD) method with adjacent cluster combining (ACC) [20], improved ED [21], contour tracing (CT) [22] or simple-signal area (S-SA) [15]. In particular, S-SA estimation can find SA accurately with lower computational cost than CT since S-SA utilizes the feature that SA is a rectangular.

However, S-SA inherently increases false alarms even though it can improve detection performance. Therefore, false alarm cancellation (FC) is added into SA estimation as a countermeasure of this problem, which is called FC+S-SA estimation [15].

In this paper, we propose computational cost efficient false alarm rejection method, L-shaped false alarm rejection (L-FAR). S-SA with L-FAR is denoted by L+S-SA

Our main contributions in this paper are summarized as follows:

- L+S-SA is proposed in this paper. L+S-SA has lower complexity than FC+S-SA. In FC+S-SA, process of FC is inserted into mid-flow of S-SA, but L-FAR is completely separated with S-SA. This structure provides an advantage in terms of computational cost at L+S-SA. Furthermore, L+S-SA estimation can achieve almost the same detection performance as FC+S-SA.
- L-shaped false alarm rejection has four parameters. It is difficult to analytically optimize L+S-SA. Therefore, we define a sub-optimization problem for L-FAR and obtain sub-optimum solution analytically. Furthermore, it is shown that the sub-optimum L+S-SA can achieve almost the same performance as the optimum L+S-SA.
- Numerical evaluations will show extensive comparison among L+S-SA, FC+S-SA and close-open+S-SA (CO+S-SA). CO is noise rejection method which is widely used in digital image processing field [23]. It will show that L+S-SA achieves the lowest computational cost and the competitive detection performance.

The reminder of this paper is as follows: process of spectrum usage detection in a spectrum sensor is provided in Section 2. Detailed process of conventional method (S-SA, FC+S-SA) and proposed method (L+S-SA) are shown in Section 3. Section 4 shows optimization and sub-optimization problem of parameters of L-FAR and derive sub-optimum parameter analytically. In Section 5, numerical results will show validity of the sub-optimum parameter and the advantage of L+S-SA in terms of computational cost. Conclusion of this paper is summarized in Section 6.

2. System Model

We focus on a process of spectrum usage detection in a spectrum sensor and a block diagram of the spectrum usage detection is shown in Fig. 1. A purpose of the spectrum usage detection is to find the occupied signal area (i.e. SA) in the observing time-frequency space.

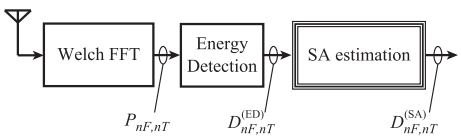

Fig. 1 Process of spectrum usage detection in spectrum sensors.

Spectrum sensors observe spectrum from $f_c - f_{sam}/2$[Hz] to $f_c + f_{sam}/2$[Hz], where f_c[Hz] is center frequency for the observation and f_{sam}[Hz] is sampling rate. The observed signal is down converted to $f_c = 0$[Hz] and the down converted signal is sampled with f_{sam}[Hz]. One observation period is

set to $N_{\rm ob}$ samples. In a *time slot*, there are N_S samples and N_S corresponds to the number of samples for single Welch FFT. Obtained samples for one observation period is divided by N_{TS} time slots where $N_{TS} = N_{\rm ob}/N_S$.

In the Welch FFT, N_S samples are divided to N_W samples with N_O overlapping samples and the N_W samples is denoted by *segment*. Then we get $N_{\rm seg}$ segments, which is given by

$$N_{\rm seg} = \frac{N_S - N_W}{N_O} + 1 = \frac{2N_S}{N_W} - 1, \tag{1}$$

where N_S and N_W are assumed to be power of 2, N_W/N_0 denotes overlap ratio which is set to 0.5 in this paper. Hamming window is applied for each segment so that we can suppress the effect of discontinuity at the boundaries of FFT frame [24]. After windowing, we perform FFT and calculate power spectrum for each segment. Estimated power spectrum in Welch FFT is given by averaging the $N_{\rm seg}$ power spectrum, and the averaging provide the gain in ED [25].

The power spectrum obtained by Welch FFT at frequency bin n_F and time slot n_T is denoted by P_{n_F,n_T} and (n_F, n_T) denotes the coordinate of tile in the observed time-frequency space. PU's bandwidth is defined by the frequency bins when the signal power is 30 [dB] below its peak value [26].

Output of ED in the tile (n_F, n_T) is denoted by $D^{(\rm ED)}_{n_F,n_T}$ and it is obtained by

$$D^{(\rm ED)}_{n_F,n_T} = \begin{cases} 1 & (P_{n_F,n_T} > \eta : \mathcal{H}_1) \\ 0 & (otherwise : \mathcal{H}_0), \end{cases} \tag{2}$$

where η is threshold of ED. $D^{(\rm ED)}_{n_F,n_T} = 1$ and $D^{(\rm ED)}_{n_F,n_T} = 0$ indicate the state of tile is estimated as $\mathcal{H}_1$ and $\mathcal{H}_0$, respectively.

SA estimation is performed to $D^{(\rm ED)}_{n_F,n_T}$ and the result is denoted by $D^{(\rm SA)}_{n_F,n_T}$. $D^{(\rm SA)}_{n_F,n_T} = 1$ and $D^{(\rm SA)}_{n_F,n_T} = 0$ means estimated occupancy state is occupied and unoccupied, respectively. Details of SA estimation is shown in Section 3. 1.

E_s/N_0 is energy per symbol to noise power spectral density ratio and defined by

$$E_s/N_0 = \frac{\sigma^2_{fS}}{2\sigma^2_{fN}} = \frac{\sigma^2_{tS}}{2\sigma^2_{tN}} \frac{f_{sam}}{B}, \tag{3}$$

where σ^2_{fS} is average signal power per unit frequency, σ^2_{fN} is average noise power per unit frequency, σ^2_{tS} is average signal power in time domain, σ^2_{tN} is average noise power in time domain and B is bandwidth of signal.

We define probability of detection $P_{\rm D}$ and probability of false alarm $P_{\rm FA}$ as metrics to evaluate the spectrum usage detection performance. $P_{\rm D}$ and $P_{\rm FA}$ for ED output are defined by

$$P^{(\rm ED)}_{\rm D} = P(D^{(\rm ED)}_{n_F,n_T} = 1 | \mathcal{H}(n_F, n_T) = \mathcal{H}_1), \tag{4}$$

$$P^{(\rm ED)}_{\rm FA} = P(D^{(\rm ED)}_{n_F,n_T} = 1 | \mathcal{H}(n_F, n_T) = \mathcal{H}_0), \tag{5}$$

respectively, where $\mathcal{H}(n_F, n_T)$ represents the actual spectrum utilization state at tile (n_F, n_T).

Given a target probability of false alarm $\dot{P}^{(\rm ED)}_{\rm FA}$, $P^{(\rm ED)}_{\rm D}$ can be approximately given by [25]:

$$\begin{aligned} P^{(\rm ED)}_{\rm D} &= \tilde{\Gamma}\left(N_{\rm seg}, \frac{\tilde{\Gamma}^{-1}\left(N_{\rm seg}, \dot{P}^{(\rm ED)}_{\rm FA}\right)}{1 + \sigma^2_{fS}/\sigma^2_{fN}}\right) \\ &= \tilde{\Gamma}\left(N_{\rm seg}, \frac{\tilde{\Gamma}^{-1}\left(N_{\rm seg}, \dot{P}^{(\rm ED)}_{\rm FA}\right)}{1 + 2E_s/N_0}\right), \end{aligned} \tag{6}$$

where $y = \tilde{\Gamma}(a, x) = (\int_x^\infty t^{a-1}e^{-t}dt)/(\int_0^\infty t^{a-1}e^{-t}dt)$ is regularized incomplete gamma function and $x = \tilde{\Gamma}^{-1}(a, y)$ is its inverse function.

We also define $P_{\rm D}$ and $P_{\rm FA}$ for SA estimation output are defined by

$$P^{(\rm SA)}_{\rm D} = P(D^{(\rm SA)}_{n_F,n_T} = 1 | \mathcal{H}(n_F, n_T) = \mathcal{H}_1), \tag{7}$$

$$P^{(\rm SA)}_{\rm FA} = P(D^{(\rm SA)}_{n_F,n_T} = 1 | \mathcal{H}(n_F, n_T) = \mathcal{H}_0), \tag{8}$$

respectively, where superscript (SA) represents a type of SA estimation method, such as S-SA.

We employ constant false alarm rate (CFAR) criterion and the design purpose of spectrum usage detection in spectrum measurement is to maximize $P^{(\rm SA)}_{\rm D}$ on the condition that $\dot{P}^{(\rm SA)}_{\rm FA} \geqq P^{(\rm SA)}_{\rm FA}$.

3. SA Estimation

3. 1 S-SA [15]

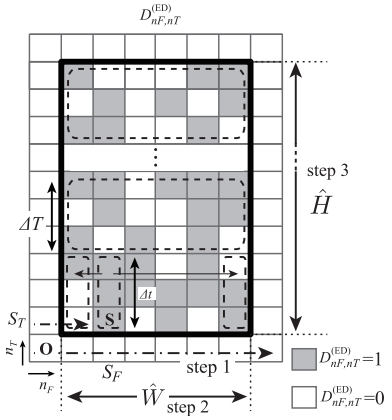

Fig. 2 S-SA estimation method.

The process of S-SA consists of three steps and an example is shown in Fig. 2. In the step 1, raster scan is performed to find a tile with $D^{(\rm ED)}_{n_F,n_T} = 1$ from origin **O** whose coordinate is $(n_F, n_T) = (0, 0)$, as shown in Fig. 2. Direction of the raster scan is left to right and bottom to top. When $D^{(\rm ED)}_{n_F,n_T} = 1$ tile is found, the tile is denoted by starting tile **S** and its coordinate is denoted by (S_F, S_T).

In the step 2, we estimate the width of SA using detection mask (dashed small rectangle in Fig. 2). Starting from **S**, the algorithm checks the detected occupancy of tiles in $n_F = S_F$ and $S_T \leqq n_T \leqq y_s + \Delta t$. If one or more of these tiles are determined as occupied, the algorithm moves to the right (n_F becomes $n_F + 1$) and repeats the process. The right edge is found when all the tiles inspected are detected as unoccupied. The left edge can be found correspondingly by moving to the opposite direction from the starting tile **S**.

In the step 3, height of SA is estimated in a similar way to step 2. Detection mask for coarse height estimation (dashed large rectangle in Fig. 2) begins with its bottom row at time slot $S_F + \Delta t + 1$ and width and height is $\hat{W}$ and ΔT, respectively. Check the number of $D^{(\mathrm{ED})}_{S_F,S_T} = 1$ tiles inside of $\hat{W}\Delta T$ detection mask, which is denoted by N. The mask is moved up by ΔT time slots and repeat the process only if $N \geqq \gamma_C \times \hat{W}\Delta T$, where γ_C is threshold. After this process, estimate the height finely and then we get the height of the SA $\hat{H}$. Details of this process has shown in [15].

As confirmed in [15], S-SA has an advantage in terms of computational cost, and it can achieve relatively good detection performance. However, S-SA increases false alarms inherently. There may be three cases increasing false alarms by S-SA and the examples are shown in Fig. 3. In the FA1, a few false alarms are adjacent and the process of step 2 in S-SA estimation causes additional false alarms by combining the tiles nearby the false alarms. In the FA2, false alarms neighbor on the left side of the SA and process of step 2 increases false alarms. In the FA3, false alarms neighbor on the bottom side of the SA and again process of step 2 increases false alarms. In all cases, area surrounded by a dotted line in Fig. 3 will be false alarms by the process of step 2.

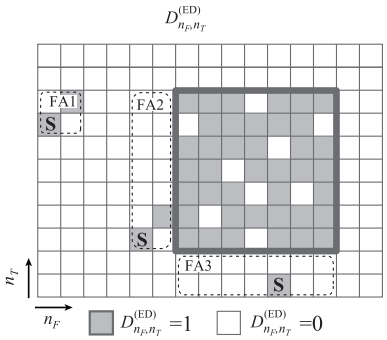

Fig. 3 False alarms caused by S-SA.

3.2 FC+S-SA

To mitigate the increment of false alarms, FC was proposed in [15]. A flow chart of FC+S-SA which corresponds to S-SA in conjunction with FC is shown in Fig. 4(a). A role of FC is re-determines the state of **S** based on two conditions and FC is performed after the step 2. If the first

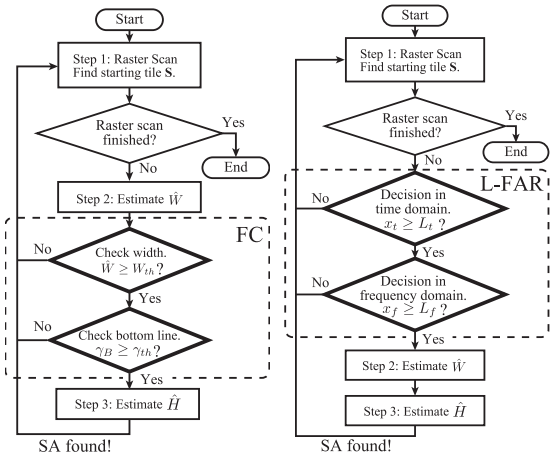

(a) FC+S-SA (b) L+S-SA

Fig. 4 Flow chart of S-SA methods. Thick flame is process of false alarm rejection such as FC or L-FAR.

condition $\hat{W} \geqq W_{th}$, where W_{th} is threshold, is not satisfied, FC determines the state of **S** as false alarm and it goes back to the raster scan (step 1). This condition can cancel false alarms with the FA1. In the second condition, the number of tiles with $D^{(\mathrm{ED})}_{n_F,n_T} = 1$ is counted at the bottom tiles of the estimated SA in the step 2. The ratio of the number and $\hat{W}$ is denoted by γ_B and if the condition $\gamma_B \geqq \gamma_{FC}$, where γ_{FC} is threshold, is not satisfied, FC determines the state of **S** as false alarm and it goes back to the raster scan (step 1). If the both conditions are satisfied, finally FC determines the state of **S** as signal component and proceeds the step 3.

3.3 L+S-SA

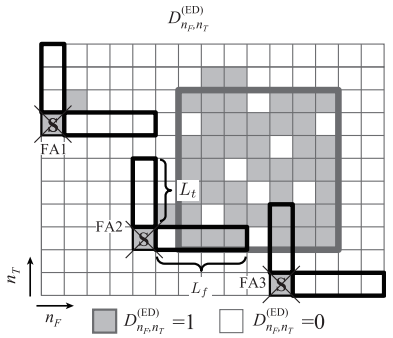

Fig. 5 Example of L-shaped false alarm removal. Parameters are set to $L_t = 3, \gamma_t = 1, L_f = 4, \gamma_f = 2$

A flow chart of L+S-SA is shown in Fig. 4(b) and example of false alarm removal by L-FAR is shown in Fig. 5. L-FAR is performed after the raster scan (step 1), therefore the process of step 2 is not necessary if the state of **S** is determined as false alarm. This can provide the benefit in terms of computational cost of the L-FAR compared to FC.

L-FAR determines state of **S** based on two conditions designed by two detection masks. The Fig. 5 shows L-FAR and

sizes of detection masks are L_f tiles in frequency domain and L_t tiles in time domain, respectively. The reason that we use L-shaped detection mask is tiles in the other directions have already investigated by the raster scan.

The condition with detection mask for frequency domain is $x_f \geqq \gamma_f$ where x_f is the number of $D^{(\mathrm{ED})}_{n_F,n_T} = 1$ tiles in the detection mask for frequency domain, and γ_f is threshold. In a similar way, the condition with detection mask for time domain is $x_t \geqq \gamma_t$ where x_t is the number of $D^{(\mathrm{ED})}_{n_F,n_T} = 1$ tiles in the detection mask for time domain, and γ_t is threshold. If one or more conditions are not satisfied, L-FAR determines the state of **S** as false alarm and it goes back to the raster scan (step 1). Otherwise, steps 2 and 3 are performed. Obviously, L-FAR can remove false alarm with the FA1 unless there are false alarms more than threshold. In addition, the L-shape detection masks can also remove the false alarms with the FA2 and FA3 since it requires that enough number of $D^{(\mathrm{ED})}_{n_F,n_T} = 1$ tiles in both domains simultaneously. In the FA2 and FA3, one of them would not satisfy the condition so its state is determined as false alarm. In addition, L-FAR tends to determine state of the tile at **S** positioned in the bottom left side of SA as signal component. This is a preferable aspect for S-SA estimation.

4. Parameter Design of L-FAR

4.1 Optimization Problems

L-FAR has four parameters, γ_t, γ_f, L_t, L_f. To simplify the optimization problem in terms of four parameters, we set $\gamma_t = 1$ and $\gamma_f = 2$. In the time domain, $D^{(\mathrm{ED})}_{n_F,n_T}$ is independent and $\gamma_t = 1$. In contrast, there are considerable correlation between $D^{(\mathrm{ED})}_{n_F,n_T}$ in the frequency domain due to the window function and the overlaps in Welch FFT, such as correlation coefficient between neighboring frequency bins is about 0.41, therefore $\gamma_f = 2$.

The optimization problem for L_t and L_f is defined by

$$\left(L_t^{(\mathrm{opt})}, L_f^{(\mathrm{opt})}\right) = \underset{L_t,L_f}{\arg\max}\, P_{\mathrm{D}}^{(\mathrm{L+S\text{-}SA})}(L_t, L_f) \qquad (9)$$
$$s.t.\;\; P_{\mathrm{FA}}^{(\mathrm{L+S\text{-}SA})}(L_t, L_f) = \dot{P}_{\mathrm{FA}}^{(\mathrm{L+S\text{-}SA})},$$

where $P_{\mathrm{D}}^{(\mathrm{L+S\text{-}SA})}(L_t, L_f)$ and $P_{\mathrm{FA}}^{(\mathrm{L+S\text{-}SA})}(L_t, L_f)$ denotes P_{D} and P_{FA} of L+S-SA output, respectively and $\dot{P}_{\mathrm{FA}}^{(\mathrm{L+S\text{-}SA})}$ denotes a target P_{FA} of L+S-SA output.

To achieve the optimization, there are two issues. The first issue is that we need to analyze ED, L-FAR and S-SA jointly to solve this optimization problem, but this is not easy. The second issue is that the optimal solution in (9) also depends on distribution of SA in the observed space, PU data traffic and specification of the transmitted signals.

For the first issue, we focus on the performance of L-FAR based on ED outputs. Based on this idea, sub-optimization problem is given by

$$\left(L_t^{(\text{sub-opt})}, L_f^{(\text{sub-opt})}\right) = \underset{L_t,L_f}{\arg\max}\, P_{\mathrm{D}}^{(\mathrm{L})}(L_t, L_f) \qquad (10)$$
$$s.t.\;\; P_{\mathrm{FA}}^{(\mathrm{L})}(L_t, L_f) = \dot{P}_{\mathrm{FA}}^{(\mathrm{L})},$$

where $P_{\mathrm{FA}}^{(\mathrm{L})}(L_t, L_f)$ and $P_{\mathrm{D}}^{(\mathrm{L})}(L_t, L_f)$ denotes P_{FA} and P_{D} of the output of model respectively and $\dot{P}_{\mathrm{FA}}^{(\mathrm{L})}$ denotes target P_{FA} at the output of L-FAR. Specifically, for a given ED outputs with an observation period, the output of L-FAR corresponds to applying L-FAR for the whole observation space without step 2 and 3.

For the second issue, we assume certain situation for the optimizations (9) and (10). This model assumes FA3 in Fig. 5.

Furthermore, most of the effect of spectral leak due to hamming window is between neighboring tiles. Therefore, we only consider correlation between neighboring tiles in the analysis.

4.2 Analysis of $P_{\mathrm{D}}^{(\mathrm{L})}$

For the second issue, the assumed situation is displayed in A of Fig. 6. Specifically, whole detection masks for L-FAR are in the SA.

For L-FAR detecting H_1 at tile (n_F, n_T), it needs to satisfy three conditions, $D^{(\mathrm{ED})}_{n_F,n_T} = 1$, and conditions of two detection masks in L-FAR are satisfied. Therefore, P_{D} is given by

$$P_{\mathrm{D}}^{(\mathrm{L})} = P(D^{(\mathrm{ED})}_{n_F,n_T} = 1) \cdot P_{\mathrm{freq}} \cdot P_{\mathrm{time}}, \qquad (11)$$

where P_{freq} denotes a probability that the condition in the detection mask of L-FAR in frequency domain is satisfied, and P_{time} denotes a probability that the condition in the detection mask of L-FAR in time domain is satisfied. The coordinate of tile with $D^{(\mathrm{ED})}_{n_F,n_T} = 1$ is set to (S_F, S_T) based on step 1.

In this case, P_{time} is given by

$$P_{\mathrm{time}} = P(x_t \geqq \gamma_t) \qquad (12)$$
$$= \sum_{k=\gamma_t}^{L_t} Bin(L_t, k, P_{\mathrm{D}}^{(\mathrm{ED})}), \qquad (13)$$

where $Bin(n, k, p) = \binom{n}{k} p^k (1-p)^{n-k}$ denotes binomial distribution, i.e. probability of k times success in n trials while each independent trial can be success with probability p, and in this case p is set by $P_{\mathrm{D}}^{(\mathrm{ED})}$.

In the case of P_{freq}, Binomial distribution is not applicable due to the non-negligible correlation of ED outputs in frequency domain. P_{freq} is given by

$$P_{\mathrm{freq}} = P(x_f \geqq \gamma_f | D^{(\mathrm{ED})}_{n_F,n_T} = 1).$$
$$= \frac{P(x_f \geqq \gamma_f, D^{(\mathrm{ED})}_{n_F,n_T} = 1)}{P(D^{(\mathrm{ED})}_{n_F,n_T} = 1)}. \qquad (14)$$

Now we focus on tiles in the detection mask for frequency domain and starting tile **S** and redefine index numbers for the tiles. Specifically, indexes for the tiles $n_F = S_F, S_F + 1, \cdots, S_F + L_f$ are redefined by $n = L_f + 1, L_f, \cdots, 1$, respectively. In addition, $D^{(\cdot)}_{n_F,n_T}$ is abbreviated to $D^{(\cdot)}_{n_F}$. In this case, the denominator in (14) is re-denoted by

$$P(x_f \geqq \gamma_f, D_{L_f+1} = 1) = \sum_{x=\gamma_f+1}^{L_f+1} P_{L_f+1}(x, D_{L_f+1} = 1). \quad (15)$$

where the suffix $L_f + 1$ of P_{L_f+1} indicates that it considers tiles in the region $1 \leqq n \leqq L_f + 1$, and x denote the number of tiles with $D_n = 1$ in the region. The term in right-hand side of (15) can be calculated recursively as follows: [27]

$$P_n(x, D_n = 1) = \sum_{d=0}^{1} P_{n-1}(x-1, D_{n-1} = d) \cdot P(D_n = 1 | D_{n-1} = d). \quad (16)$$

Considering the correlation between neighboring tiles, the conditional probability at second term in the right side in (16) can be obtained by

$$P(D_n | D_{n-1}) = \left(P_{\mathrm{D}}^{(\mathrm{ED})}(1 - \rho_S^{(\mathrm{ED})}) + \rho_S^{(\mathrm{ED})} D_{n-1}\right)^{D_n} \cdot \left(\left(1 - P_{\mathrm{D}}^{(\mathrm{ED})}\right)(1 - \rho_S^{(\mathrm{ED})}) + \rho_S^{(\mathrm{ED})}(1 - D_{n-1})\right)^{1-D_n}, \quad (17)$$

where $\rho_S^{(ED)}$ is correlation coefficient of ED outputs between the neighboring tiles at inside of SA. The initial value of (16) ($n = 1$) is defined by

$$P_1(x, D_1 = d) = \begin{cases} P_{\mathrm{D}}^{(\mathrm{ED})} & (x = 1, d = 1) \\ 1 - P_{\mathrm{D}}^{(\mathrm{ED})} & (x = 0, d = 0). \end{cases} \quad (18)$$

Note that $x = 0$ and $d = 1$, or $x = 1$ and $d = 0$ will not be occurred.

4.3 Analysis of $P_{\mathrm{FA}}^{(\mathrm{L})}$

For the second issue, the area surrounded by dotted line B in Fig. 6 is assumed for the analysis of $P_{\mathrm{FA}}^{(\mathrm{L})}$. Specifically, **S** is located below SA and L-shaped region is overlapped with SA. In addition, length in time domain of assumed area in noise area is set to N_{noise} tiles and length in time domain of assumed area in signal area is $L_t - 1$ tiles. P_{FA} is given by

$$P_{\mathrm{FA}}^{(\mathrm{L})} = P(D^{(\mathrm{ED})}_{n_F,n_T} = 1) \cdot P_{\mathrm{freq}} \cdot P_{\mathrm{time}}. \quad (19)$$

In this case, P_{time} is given by averaging over the assumed area in time domain as:

$$P_{\mathrm{time}} = P(x_t \geqq \gamma_t) = \frac{1}{N_{\mathrm{noise}} + 1} \sum_{k=0}^{N_{\mathrm{noise}}} \sum_{x_t=\gamma_t}^{L_t} P(x_t \geqq \gamma_t | k, L_t - k), \quad (20)$$

where k indicates the number of time domain tiles of L-shaped region in noise area, and $L_t - k$ indicates the number of time domain tiles of L-shaped region in signal area. Specifically, k determines the location of L-shaped region in the assumed area. In addition, $P(x_t \geqq \gamma_t | k, L_t - k)$ is given by

$$P(x_t \geqq \gamma_t | k, L_t - k) = \begin{cases} \sum_{l=0}^{x_t} Bin(k, l, P_{\mathrm{FA}}^{(\mathrm{ED})}) \cdot Bin(L_t - k, x_t - l, P_{\mathrm{D}}^{(\mathrm{ED})}) & (k \leq L_t) \\ Bin(L_t, x_t, P_{\mathrm{FA}}^{(\mathrm{ED})}) & (otherwise). \end{cases} \quad (21)$$

P_{freq} can be obtained by the similar way (14)-(18), but replace $P_{\mathrm{D}}^{(\mathrm{ED})}$ and $\rho_S^{(\mathrm{ED})}$ with $P_{\mathrm{FA}}^{(\mathrm{ED})}$ and $\rho_N^{(\mathrm{ED})}$, respectively where $\rho_N^{(ED)}$ is correlation coefficient of ED result between neighboring frequency tiles in the noise area.

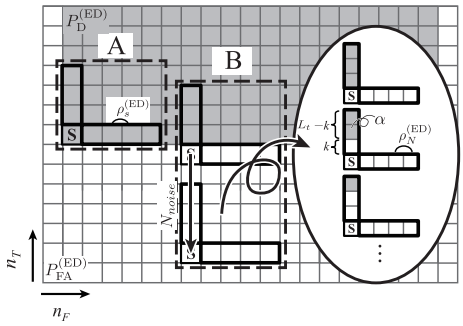

Fig. 6 Derivation of $P_{\mathrm{D}}^{(\mathrm{L})}$ and $P_{\mathrm{FA}}^{(\mathrm{L})}$ based on analysis model. We focus on the bottom side of SA and correlation is considered only neighboring tiles.

5. Numerical Evaluations

Table 1 Simulation parameters for each SA estimation methods.

FFT size (N_S)	2^{10}
segment size (N_W)	2^7
overlap ratio (N_W/N_O)	0.5
window function	hamming window
$\dot{P}_{\mathrm{FA}}^{(\mathrm{SA})}$	0.01
sampling rate[MHz]	40
band width of PU signal[MHz]	20
duration of one packet[us]	256
idle time[us]	205

In this section, we evaluate validity of sub-optimization of L+S-SA and compare the detection performances among L+S-SA and conventional methods (FC+S-SA, CO+S-SA) based on CFAR criterion. Common simulation parameter setting is shown in Table 1.

5.1 Sub-optimization of L+S-SA

Fig. 7 shows obtained L_t and L_f as a function of E_s/N_0

for different methods. $L_t^{(\text{sub-opt analysis})}, L_f^{(\text{sub-opt analysis})}$ denotes the analytically obtained sub-optimal solution (10), $L_t^{(\text{sub-opt})}, L_f^{(\text{sub-opt})}$ denotes the sub-optimal solution based on Monte Carlo simulation, and $L_t^{(\text{opt})}, L_f^{(\text{opt})}$ denotes the optimal solution (9) based on Monte Carlo simulation.

Sub-optimal solution is based on analysis model of Fig. 6 and N_{noise} is set to 10.

In terms of sub-optimization, analytical result agrees with the result of Monte Carlo simulation and it shows the validity of analysis. On the other hand, there is difference between the sub-optimal solution and the optimal solution and it is at most four. In addition, the difference increases as E_s/N_0 increases. Next, we will confirm an effect of this difference in terms of detection performance.

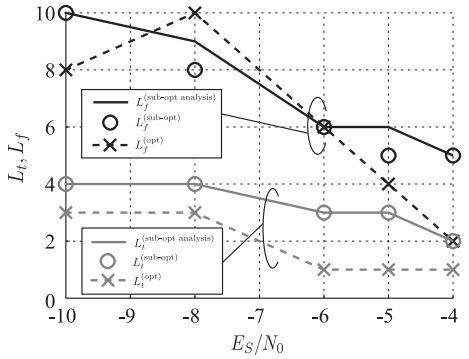

Fig. 7 Comparison of derived parameters by each methods. γ_t is fixed to 1 and γ_f is fixed to 2. $\dot{P}_{\text{FA}}^{(\text{L})} = 0.01$.

5.2 Detection Performances

Fig. 8 shows detection probability as a function of E_s/N_0 in terms of L+S-SA with several parameter setting solutions, FC+S-SA, CO+S-SA in which closing-opening is used for false alarm rejection [23], ans S-SA. As confirmed in Fig. 7, proper L_t and L_f depends on E_s/N_0, but it is difficult to adjust them with E_s/N_0. Therefore we also show a result denoted by "analytical fixed" in Fig. 8 and in this result, analytically obtained sub-optimal solution when $E_s/N_0 = -6$ dB is used in the whole E_s/N_0 region. The reason of $E_s/N_0 = -6$ dB is that P_{D} achieves 0.9.

In L+S-SA, this result indicates that at least the optimal solution can achieve the highest detection probability, but the difference among optimization solutions is negligible. Also, L+S-SA can achieve almost the same performance as FC+S-SA. On the other hand, we can confirm that L+S-SA can achieve better detection probability compared to CO+S-SA in the region where E_s/N_0 is more than -8 [dB].

5.3 Computational Time

Fig. 9 shows computational time as a function of $P_{\text{FA}}^{(\text{SA})}$. CO+S-SA needs a lot of computational time.

L+S-SA and FC+S-SA needs more computational time

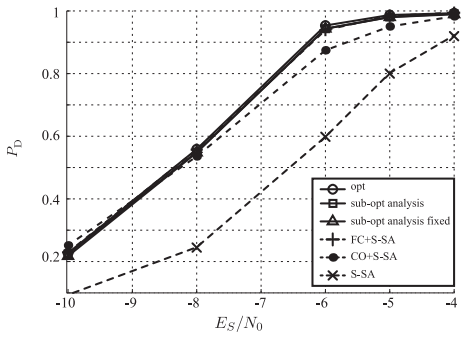

Fig. 8 Detection probability of SA estimation methods.

than S-SA due to false alarm rejection. L+S-SA has lower computational cost than FC+S-SA because L+S-SA can remove false alarm tile before S-SA process, while FC+S-SA make decision after width estimation of S-SA (step 2).

In Fig. 9, computational time of L+S-SA and FC+S-SA is minimum around $P_{\text{FA}}^{(\text{SA})}$=0.004. Computational time depends on the number of $D_{n_F,n_T}^{(\text{ED})} = 1$ tiles found by raster scan. Fig. 10 shows N_{noise} and N_{signal} where N_{noise} denotes number of tiles denoted as false alarm by FC or L-FAR and N_{signal} denotes number of tiles denoted as signal by FC or L-FAR. Computational cost depends on $N_{\text{noise}} + N_{\text{signal}}$ because we conduct S-SA process for every $D_{n_F,n_T}^{(\text{ED})} = 1$ tiles found by raster scan.

If $P_{\text{FA}}^{(\text{SA})}$ is very low (lower than 0.004 in Fig. 9), there are a few false alarms tiles. But detection probability is also very low. Therefore, tiles will be denoted as noise even if it is inside of SA. Therefore, N_{noise} and computational time will be increased.

If $P_{\text{FA}}^{(\text{SA})}$ is very high (higher than 0.004 in Fig. 9), there are a lot of false alarm tiles and computational time will be increased.

In the middle region (around 0.004 in Fig. 9), SA can be found by minimum number of rectangle and number of S-SA process is minimized. Therefore computational time takes minimum value.

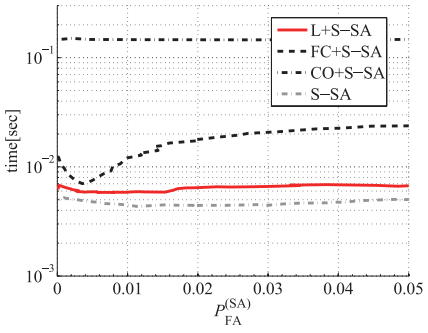

Fig. 9 computational time of SA estimation methods. ($E_s/N_0 = -5$[dB])

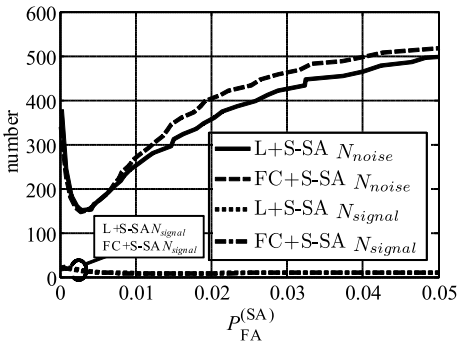

Fig. 10 Number of signal tiles N_{signal} and number of noise tiles N_{noise} over 1 observation period. ($E_s/N_0 = -5$[dB])

6. Conclusion

In this paper, we investigated false alarm rejection method for S-SA estimation which is post process of ED. We have proposed L-FAR which is accurate and low computational time than conventional methods.

Also, we proposed sub-optimum parameter setting method based on analysis model of L+S-SA. Considering process of L+S-SA, its performance can be analyzed only considering L-FAR around the bottom side of SA. In addition, assuming correlation exists only between neighboring ED outputs in frequency domain, we can analytically calculate P_{D} and P_{FA}. We can design sub-optimum parameters analytically by this analysis.

Furthermore, simulation results show sub-optimum parameter can achieve almost the same detection performance as optimum parameters, and proposed method (L+S-SA) can achieve competitive detection performance to FC+S-SA while lower computational time.

文　献

[1] FCC, "Spectrum Policy Task Force ET Dcket No. 02-135," 2002.

[2] I. F. Akyildiz, W.-Y. Lee, M. C. Vuran, and S. Mohanty, "NeXt generation/dynamic spectrum access/cognitive radio wireless networks: A survey," *Computer Networks*, vol. 50, no. 13, pp. 2127–2159, 2006.

[3] L. Lu, X. Zhou, U. Onunkwo, and G. Li, "Ten years of research in spectrum sensing and sharing in cognitive radio," *EURASIP Journal on Wireless Communications and Networking*, no. 1, p. 28, 2012.

[4] J. Lunden, V. Koivunen, and H. Poor, "Spectrum Exploration and Exploitation for Cognitive Radio," *IEEE Signal Process. Mag.*, vol. 32, no. 3, pp. 123–140, 2015.

[5] T. Yucek and H. Arslan, "A survey of spectrum sensing algorithms for cognitive radio applications," *IEEE Commun. Surveys Tuts.*, vol. 11, no. 1, pp. 116–130, 2009.

[6] H. O. Kpojime and G. A. Safdar, "Interference Mitigation in Cognitive-Radio-Based Femtocells," *IEEE Commun. Surveys Tuts.*, vol. 17, no. 3, pp. 1511–1534, jan 2015.

[7] J. J. Lehtomäki, R. Vuohtoniemi, and K. Umebayashi, "On the Measurement of Duty Cycle and Channel Occupancy Rate," *IEEE Journal on Selected Areas in Communications*, vol. 31, no. 11, pp. 2555–2565, nov 2013.

[8] N. Wang, Y. Gao, and X. Zhang, "Adaptive spectrum sensing algorithm under different primary user utilizations," *IEEE Commun. Lett.*, vol. 17, no. 9, pp. 1838–1841, 2013.

[9] T. Nguyen, B. L. Mark, and Y. Ephraim, "Spectrum sensing using a hidden bivariate markov model," *IEEE Trans. Wireless Commun.*, vol. 12, no. 9, pp. 4582–4591, 2013.

[10] D. Zhao and X. Zhou, "Spectrum Sensing Using Prior Probability Prediction," in *Proc. WiCOM*, 2011, pp. 1–4.

[11] J. Vartiainen and H. Marko, "Priority Channel Selection Based on Detection History Database," in *in Proc. CROWNCOM*, 2010, pp. 1 – 5.

[12] K. Umebayashi and Y. Suzuki, "Dynamic selection of CWmin in cognitive radio networks for protecting IEEE 802.11 primary users," in *Proc. CROWNCOM*, 2011, pp. 266 – 270.

[13] Y. Xu, A. Anpalagan, Q. Wu, L. Shen, Z. Gao, and J. Wang, "Decision-Theoretic Distributed Channel Selection for Opportunistic Spectrum Access: Strategies, Challenges and Solutions," *IEEE Commun. Surveys Tuts.*, vol. 15, no. 4, pp. 1689–1713, jan 2013.

[14] K. Umebayashi, S. Tiiro, and J. Lehtomäki, "Development of a measurement system for spectrum awareness," in *Proc. 5GU*, 2014.

[15] K. Umebayashi, K. Moriwaki, R. Mizuchi, H. Iwata, S. Tiiro, J. J. Lehtomäki, M. López-Benítez, and Y. Suzuki, "Simple Primary User Signal Area Estimation for Spectrum Measurement," *IEICE Trans. Commun.*, vol. E99-B, no. 02, 2016.

[16] H. Urkowitz, "Energy detection of unknown deterministic signals," *Proc. IEEE*, vol. 55, no. 4, 1967.

[17] Qiwei Zhang, A. B. Kokkeler, and G. J. Smit, "An efficient multi-resolution spectrum sensing method for cognitive radio," in *Proc. CHINACOM*, 2008, pp. 1226–1229.

[18] P. Welch, "The use of fast Fourier transform for the estimation of power spectra: A method based on time averaging over short, modified periodograms," *IEEE Trans. Audio Electroacoust.*, vol. 15, no. 2, pp. 70–73, 1967.

[19] K. Umebayashi, R. Takagi, N. Ioroi, J. Lehtomäki, and Y. Suzuki, "Duty cycle and noise floor estimation with Welch FFT for Spectrum Usage Measurements," *Proc. CROWNCOM*, 2014.

[20] J. Vartiainen, H. Sarvanko, J. Lehtomäki, M. Juntti, and M. Latva-aho, "Spectrum Sensing with LAD-Based Methods," in *Proc. PIMRC*, 2007, pp. 1–5.

[21] M. López-Benítez and F. Casadevall, "Improved energy detection spectrum sensing for cognitive radio," *IET Communications*, vol. 6, no. 8, p. 785, 2012.

[22] J. Kokkoniemi and J. Lehtomaeki, "Spectrum Occupancy Measurements and Analysis Methods on the 2.45 GHz ISM Band," in *Proc. CROWNCOM*, 2012.

[23] P. Soille, *Morphological Image Analysis*. Springer Berlin Heidelberg, 2004.

[24] A. V. Oppenheim and R. W.Schafer, *Discrete-Time Signal Processing 3rd Edition*. Pearson Education, 2013.

[25] H. Iwata, K. Umebayashi, S. Tiiro, Y. Suzuki, and J. J. Lehtomäki, "Optimum welch FFT segment size for duty cycle estimation in spectrum awareness system," in *Proc. WCNCW*, mar 2015, pp. 229–234.

[26] ITU-R, "SPECTRA AND BANDWIDTH OF EMISSIONS," *RECOMMENDATION ITU-R SM.328-10*, 1999.

[27] S. Mori and M. Hisakado, "Correlated binomial model on networks," *Transactions on Mathematical Modeling and its Applications, Information Processing Society of Japan*, vol. 2, no. 1, pp. 22–36, 2009.